

PROMINENCE MAGNETIC DIPS IN THREE-DIMENSIONAL SHEARED ARCADES

G. AULANIER

Observatoire de Paris, Laboratoire d'Etudes Spatiales et d'Instrumentation en Astrophysique, 92195 Meudon Cedex, France

C. R. DEVORE

Naval Research Laboratory, Laboratory for Computational Physics and Fluid Dynamics, Code 6440, Washington, DC 20375

AND

S. K. ANTIOCHOS

Naval Research Laboratory, Solar-Terrestrial Relationships Branch, Code 7675, Washington, DC 20375

Received 2001 October 10; accepted 2002 January 3; published 2002 February 8

ABSTRACT

We calculate the distribution of field-line dips in the three-dimensional sheared arcade model for prominence/filament magnetic fields. We consider both moderately and highly sheared configurations computed by fully time-dependent three-dimensional MHD simulations in which the field was relaxed to a static equilibrium end state. In agreement with previous low spatial resolution measurements of the magnetic field inside prominences, we find that for all configurations, the field in the great majority of the calculated dips exhibits inverse polarity. But for each configuration we also find well-defined narrow regions with stable dips of normal polarity. These tend to be located on the edges of the filament ends and at the top of the central part of the prominence. This distinctive mixture of normal/inverse polarity dips that we find in sheared arcades is not likely to be present in twisted flux rope prominence models. Therefore, our results provide a rigorous and unique observational test that can distinguish between the two classes of models, as well as new predictions for future high spatial resolution spectropolarimetric observations of filaments and prominences.

Subject headings: MHD — Sun: filaments — Sun: magnetic fields — Sun: prominences

1. INTRODUCTION

The magnetic fields of prominences/filaments (or more generally, filament channels) are widely believed to play the determining role in eruptive flares and coronal mass ejections (see, e.g., Mikić & Linker 1994; Forbes, Priest, & Isenberg 1994; Antiochos, DeVore, & Klimchuk 1999; Amari et al. 2000). Prominence magnetic fields are also likely to provide key insights into understanding coronal heating (Poland & Mariska 1986; Antiochos, MacNeice, & Spicer 2000) and the helicity budget of the Sun (Low 1996; Démoulin et al. 2002). Consequently, determining the magnetic structure of prominences has long been one of the outstanding problems in solar physics (e.g., Tandberg-Hanssen 1995).

The main constraint derived from years of observations is that the prominence magnetic field must be capable of supporting against gravity the cool dense material overlying a photospheric neutral line (e.g., Tandberg-Hanssen 1995). This leads naturally to theoretical models that involve field-line dips in a bipolar magnetic system (see the review of models by Démoulin 1998). Most of these models fall into two broad classes: the sheared three-dimensional arcades (Antiochos, Dahlburg, & Klimchuk 1994; DeVore & Antiochos 2000) and the twisted flux ropes (e.g., Malherbe & Priest 1983; Aulanier & Démoulin 1998; Amari et al. 1999; van Ballegoijen, Priest, & MacKay 2000). An intense debate has raged in the literature over which of these two models (if either) is correct, in large part because the structure of prominence magnetic fields has profound implications for theories of coronal mass ejections and eruptive flares (e.g., reviews by Forbes 2000; Klimchuk 2001; Low 2001). An observational test that will decisively discriminate between the two models is clearly needed.

Fortunately, the cool mass of a prominence is the one location in the corona where it is possible to make direct measurements of the magnetic field with the Zeeman and Hanle effects (Rust 1967; Nikolskii et al. 1984; Leroy, Bommier, &

Sahal-Bréchet 1983; Bommier et al. 1994). The latter have shown that the magnetic field is nearly horizontal, it makes on average an angle of 10° – 40° with the filament axis, and its magnitude tends to increase with height. Using several techniques to solve the 180° ambiguity for the orientation of transverse fields observed with a $5''$ spatial resolution, Bommier (1998) has reported that about 90% of prominences have an inverse polarity (IP) configuration: the field component perpendicular to the body of the prominence is directed opposite to what a potential field would predict. The few other prominences that were found to have a normal polarity (NP) were located mainly in active regions and had low vertical extent (Leroy, Bommier, & Sahal-Bréchet 1984). Nikolskii, Kim, & Koutchmy (1982) and Kim (1990) obtained measurements with $3''$ – $8''$ spatial resolution of several prominences that exhibited mixtures of $B_{\parallel} > 0$ and $B_{\parallel} < 0$. But owing to a lack of knowledge of the prominence geometry and since only the line-of-sight component of the magnetic field was measured, it is unclear whether these observations imply mixtures of NP and IP.

In this Letter we argue that the measurement of prominence polarity can be a decisive test of prominence models. The key point is that for the standard twisted flux rope models, in which the field lines undergo at least one turn in the corona, the dips should be either all IP, if a null point occurs below the rope as in the classical Kuperus-Raadu (1974) configuration, or all NP, if the null point occurs above the rope (Malherbe & Priest 1983; Démoulin & Forbes 1992). We show that although the three-dimensional arcade models are primarily IP, they have well-defined regions that are NP. Our results imply that this mixture of IP and NP is an intrinsic property of three-dimensional sheared arcades and, hence, is a clear discriminator between this model and twisted flux ropes. We also discuss several other important predictions of the sheared arcade model and the interpretation of prominence observations.

2. THE SHEARED ARCADE MODEL

We used our explicit flux-corrected transport MHD code to calculate a number of three-dimensional sheared arcade solutions, as in DeVore & Antiochos (2000, hereafter DA2000). The computational box consisted of the domain $x \in [-24, 24]$, $y \in [-6, 6]$, $z \in [0, 12]$, with a grid $n_x n_y n_z = 500 \times 190 \times 190$ that was nonuniform (stretched exponentially from the origin). The initial condition for all runs was that of a field due to a point dipole of strength $B = 4$ oriented along y , located at $z = -2$, and embedded in a uniform atmosphere of $p = 10^{-2}$. Open boundary conditions were assumed for the top plane ($z = 12$) and all side walls, while rigid-wall, line-tied conditions with a prescribed shear flow were used at the photosphere ($z = 0$). This flow was parallel to and localized about the neutral line, $y = 0$, and produced a displacement of the form $X = (D/\pi) [\pi t/t_E - \sin(\pi t/t_E)] \sin(\pi y)$ for $|y| \leq 1$ and $0 \leq t \leq t_E$, and $X = 0$ otherwise. In order to model prominences formed under different conditions, we performed two separate calculations: a small (S) and a large (L) footpoint shearing, with displacement amplitudes of $D(S) = 6$ and $D(L) = 16$.

We took particular care in the present study to obtain true equilibrium solutions; consequently, we evolved the field 2 times slower than in DA2000 by applying an average photospheric velocity that was only 8% of the coronal Alfvén speed. Furthermore, after the end of the shearing phase t_E , we let the field relax for a longer time, until the time t_F , which was chosen so that the final integrated kinetic energy was $\approx 10\%$ of its maximum value throughout the evolution (see Fig. 1). We used $[t_E; t_F](S) = [75; 300]$ and $[t_E; t_F](L) = [200; 600]$.

At $t = t_F$, some waves were still propagating along some long field lines (see the overlying potential loops on Fig. 2). Since these waves occurred in only weak field regions, they did not have a significant effect on the magnetic energy. Such waves take a very long time to damp with our explicit scheme and high numerical resolution and are likely to be present in real prominences, so we did not attempt to eliminate them. Their effect on the formation of transient dips in flattened field lines is discussed in § 3.

3. CALCULATION OF MAGNETIC DIPS

Most prominence theoretical models assume that magnetic dips are required to support cool condensations against gravity. Even though this issue is still debated (by, e.g., Zirker, Engvold, & Martin 1998 and Karpen et al. 2001), we adopted the standard assumption that cool prominence material occurs on only dipped field lines and rests stably in the first scale height from the bottom of the dip. Note that the qualitative results derived below are likely to remain valid even if all cool prominence material is dynamic along the dips.

We chose a spatial scaling in (x, y, z) such that one unit of distance in our computational domain corresponds to 20 Mm. The distribution of magnetic dips was calculated using the same procedure as in Aulanier, Srivastava, & Martin (2000), using a sampling of $\Delta x = 12$ Mm and $\Delta y = \Delta z = 2$ Mm. We have checked that the results are not changed by using a finer sampling. Since the neutral line remains at $y = 0$ throughout the evolution, the polarity (NP vs. IP) of each dip is determined directly by the sign of B_y .

For both the S and L cases, we identified a few groups of dips located far from the main distribution (see § 4). From analysis of the MHD solutions for $t < t_F$, we found that most of these isolated dips become more and more shallow with time, with the majority disappearing prior to a time of $t =$

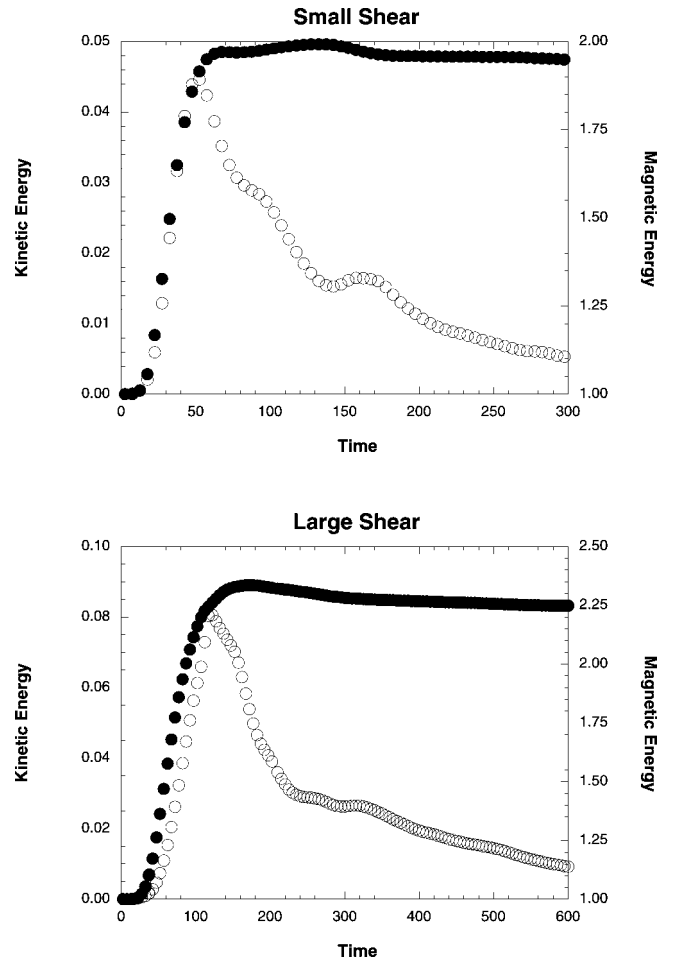


FIG. 1.—Magnetic (*filled circles*) and kinetic (*open circles*) energies as a function of time for the small (S) and large (L) shear cases.

$0.7t_F$. Some of these dips are located in the overlying unsheared field lines, but most are associated with sheared field lines that are very flat and that are produced by reconnection between the sheared core field and the potential loops (see DA2000 for details). For these reasons we believe that these isolated dips are not relevant to observations but are an artifact of propagating waves that are not sufficiently damped by our code and/or of field lines that have not yet fully relaxed. The field magnitude in these dips is small at $t = t_F$, $B \leq 0.4$, while in the main distribution, $B \geq 0.6$. Hence, in order to eliminate these spurious dips, which would require prohibitive computer time to relax away, we have only calculated dips for which $B \geq 0.5$. The resulting distributions of dips for S and L at $t = t_F$ are plotted in Figure 2.

4. COMPARISON OF SMALL AND LARGE SHEAR CASES

Although the S and L configurations show differences, they share many properties. In accordance with observations, the simulated prominences are well aligned with the neutral line along the x -axis. Their height decreases smoothly from the center [$H(x = 0) \approx 30$ Mm] toward the ends. Owing to the inhomogeneous photospheric distribution of B_z and of the force-free parameter $\alpha = \mathbf{j} \cdot \mathbf{B}/B^2$, the dips form a complex structure that is not as smooth as that obtained with flux rope models, even when the latter are perturbed by small-scale parasitic polarities at the photosphere (see Aulanier et al. 2000 for comparison).

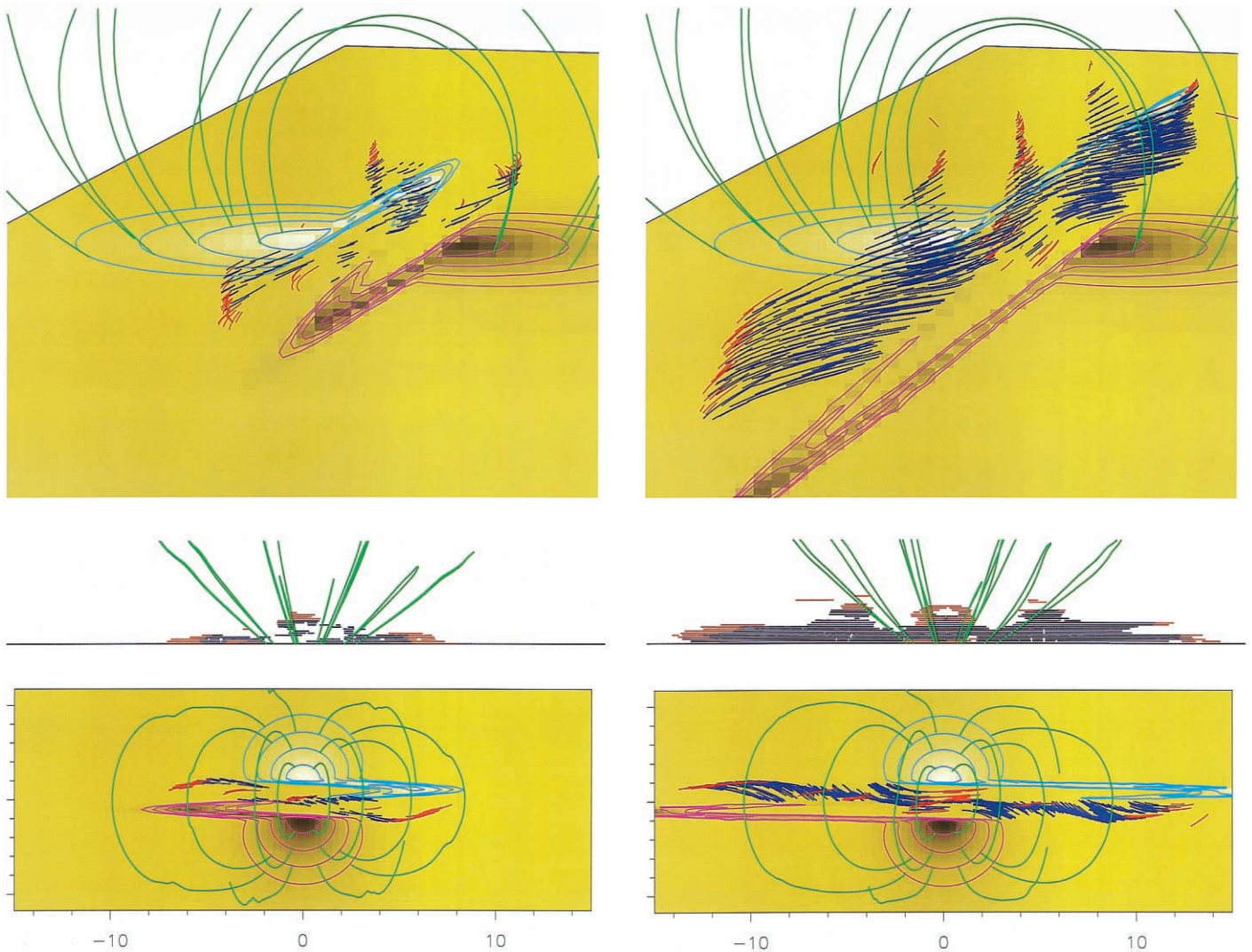


FIG. 2.—Distribution of NP (red) and IP (dark blue) magnetic dips in sheared arcs surrounded by potential loops (green). Pink and light blue contours, as well as the black-yellow-white color table, correspond to the distribution of $B_z(z=0)$. Left column: Corresponding to the *S* case; right column: corresponding to the *L* case. Top row: View in projection; middle row: view on the side as for a prominence on the limb; bottom row: view from the top as for a filament at disk center.

Most of the calculated dips have IP. There is a noticeable difference between the calculations in the orientation θ of the magnetic field in these dips with respect to the neutral line (the x -axis): $\theta(S) \approx 10^\circ\text{--}25^\circ$ and $\theta(L) \approx 20^\circ\text{--}45^\circ$, with the maximum values occurring around $|x| \approx D/2$. It may appear counterintuitive that the small shear case *S* would be more aligned with the neutral line than the large shear case *L*. The explanation is that for *S*, the magnetic topology is that of a simple sheared arcade, whereas for *L*, reconnection modifies the topology into a sheared core surrounded by a thin region of weakly helically twisted (≈ 1.5 turn) field (see DA2000).

Contrary to previous prominence models, we find that in addition to the dominant distribution of IP dips, there exist well-defined narrow regions with dips of NP. These are mainly located (1) at the top of the central part of the prominence and (2) on the edges of the filament ends. The NP dips are weakly normal, with inclination angles of $\theta \leq 5^\circ$, but they do not appear to be due to unrelaxed field lines since they do not evolve significantly from earlier times to $t = t_f$.

For the small shear case, one principal vertical column of dips is found, centered at $x = 0$, with low-lying dipped regions

near the ends of the structure. For the large shear case, there are two additional columns of dips, around $|x| = 80$ Mm (see Fig. 2, middle row). These regions also possess NP dips at their tops and are located at the edges of the central dipole. The restraining tension from the overlying unshaped fields is very weak there, and the helically twisted field is most developed. The first condition naturally allows the highly stressed fields below to rise in altitude. However, neither of these conditions obtains in the small shear case, which presumably accounts for it being devoid of a similar three-column structure.

The occurrence of NP dips in region 1 near $x = 0$ is perhaps the most important result of our work because this feature is present in all cases and it should be straightforward to observe. We find that differential shear at the photosphere naturally leads to a gradual rotation of B_y with z at the center of the bipole, $x = 0$. At low altitude z , the magnetic field configuration must be approximately that of a two-dimensional sheared arcade, implying that $B_y > 0$ (i.e., NP) with no dips. At intermediate z , the finite size of the bipole begins to take effect so that dips develop, and the three-dimensional bending of the field leads to a sigmoid shape with $B_y < 0$ (IP) at the dip (see Antiochos

et al. 1994). At still higher z , both the dips and the IP must disappear as the field becomes that of the unsheared overlying arcade; however, we find that in all cases, the three-dimensional bending tends to decrease faster with height than the dipping, so a region of NP dips forms at the top layer of the shear zone. It should be emphasized that we also find this result for the fields obtained in our previous force-free calculations (Antiochos et al. 1994), which assume a different shape for the shear profile at the photosphere. Hence, we believe this is a persistent and universal feature of the sheared three-dimensional arcade model.

A similar spatial variation is found in region 2, near the prominence ends. Since essentially all the flux there is highly sheared, there is a transition from a dipped and bent (IP) sheared field to an undipped and relatively straight (NP) sheared field. In the large shear case, many of these field lines have only one footpoint at the prominence end, with the other located near the center of the system owing to reconnection between the sheared core field and the overlying arcade (see DA2000). The result is a much more complex field geometry. In analogy with region 1, we find that with increasing $|x|$, the bending of the field decreases faster than the dipping so that a locus of NP dips forms at the prominence ends.

5. IMPLICATIONS FOR OBSERVATIONS

An important conclusion of our work is that the sheared arcade model yields a complex three-dimensional distribution of magnetic dips, with many of the general properties of observed prominences. Most of the dips are very shallow, and they tend to form along several curved vertical surfaces. Consequently, interpreting the geometry of fine structures (and plasma flows), observed, for example, in absorption in $H\alpha$ or in extreme-UV, can be very challenging because of projection effects. Although the small and large shear cases do exhibit some differences in their structure, these are due mainly to the effects of reconnection between the sheared and external field in the large shear case, which creates an envelope of weakly twisted field surrounding a core of sheared field. Nevertheless, both cases show the same basic pattern, which appears to be an intrinsic property of the sheared arcade model: (1) a mixture of magnetic dips of the IP and NP polarity types, largely dominated by the IP, and (2) small but distinct areas of NP dips, located at the top of the central part and on the edges of both ends of the prominence.

This mixture of IP/NP dips is in sharp contrast to what is expected from the twisted flux rope model for solar prominences. These would generally be expected to have either all IP or all NP dips, depending on the orientation of the rope with respect to the background field (Malherbe & Priest 1983; Démoulin & Forbes 1992). It may be possible for a twisted flux rope to contain a mixture of IP and NP dips, but only if it is

strongly perturbed, for example, by high-amplitude waves or by parasitic photospheric polarities with strong flux. Such a mixture of polarities would not be an intrinsic property of the flux rope; the timescales on which the minor polarity dips would form and disappear are likely to be much shorter than the lifetime of the prominence itself. Thus, even if three-dimensional twisted flux rope models with a mixture of IP and NP dips are constructed, it is highly unlikely that such models would exhibit a polarity distribution similar to that in Figure 2. Hence, our results constitute a clear observational signature that can be used to test the sheared three-dimensional arcade model and to discriminate decisively between this model and the twisted flux rope models.

It is unlikely, however, that the prominence observations presently available have sufficient spatial resolution and sensitivity to test the models. Most measurements showing IP have been done with a few arcsecond resolution, in the central regions of prominences, often using averages from several points in order to enhance the signal (V. Bommier 2001, private communication). Some NPs have been reported in low-lying prominences (Leroy et al. 1984), but since the latter were partially occulted by a coronagraph, only their upper portions were observed. Even though the NP at the top of prominences are consistent with the sheared arcade models, a definite association is clearly limited by the observational bias caused by the coronagraph. There have been a few measurements of the spatial distribution of prominence polarity that show a mixture of IP and NP (Nikolskii et al. 1982; Kim 1990), but these are certainly not definitive (see § 1). Therefore, new prominence magnetic field observations that will not have the above limitations are clearly needed.

In addition to the spatial distribution of IP and NP dips, we have calculated the variation of the angle between the field and the neutral line along the filament axis for the sheared arcade models. These results also provide new quantitative predictions for observations. We expect these predictions to be tested in the near future with high spatial resolution observations of filaments and prominences, both in imagery (e.g., in $H\alpha$ or in extreme-UV with *Solar-B*) and especially in spectropolarimetry with highly sensitive, new-generation instruments, such as the THEMIS, for which Paletou et al. (2001) have recently shown the ability to measure prominence magnetic fields.

The numerical calculations were performed using grants from the Department of Defence's High Performance Computing Modernization Program. G. A. wishes to thank the Naval Research Laboratory group for travel funding as well as for warm hospitality during his visits. The work of G. A. was funded by the Centre National d'Etudes Spatiales. The work of C. R. D. and S. K. A. was funded by NASA and the Office of Naval Research.

REFERENCES

- Amari, T., Luciani, J.-F., Mikić, Z., & Linker, J. 1999, *ApJ*, 518, L57
 ———. 2000, *ApJ*, 529, L49
 Antiochos, S. K., Dahlburg, R. B., & Klimchuk, J. A. 1994, *ApJ*, 420, L41
 Antiochos, S. K., DeVore, C. R., & Klimchuk, J. A. 1999, *ApJ*, 510, 485
 Antiochos, S. K., MacNeice, P. J., & Spicer, D. S. 2000, *ApJ*, 536, 494
 Aulanier, G., & Démoulin, P. 1998, *A&A*, 329, 1125
 Aulanier, G., Srivastava, N., & Martin, S. F. 2000, *ApJ*, 543, 447
 Bommier, V. 1998, in *IAU Colloq. 167, New Perspectives on Solar Prominences*, ed. D. Webb, D. Rust, & B. Schmieder (ASP Conf. Ser. 150; San Francisco: ASP), 434
 Bommier, V., Landi Degl'Innocenti, E., Leroy, J. L., & Sahal-Bréchet, S. 1994, *Sol. Phys.*, 154, 231
 Démoulin, P. 1998, in *IAU Colloq. 167, New Perspectives on Solar Prominences*, ed. D. Webb, D. Rust, & B. Schmieder (ASP Conf. Ser. 150; San Francisco: ASP), 386
 Démoulin, P., & Forbes, T. G. 1992, *ApJ*, 387, 394
 Démoulin, P., Mandrini, C. H., van Driel-Gesztelyi, L., Thompson, B. J., Plunkett, S., Kővári, Z., Aulanier, G., & Young, A. 2002, *A&A*, 382, 650
 DeVore, C. R., & Antiochos, S. K. 2000, *ApJ*, 539, 954
 Forbes, T. G. 2000, *J. Geophys. Res.*, 105, 23,153

- Forbes, T. G., Priest, E. R., & Isenberg, P. A. 1994, *Sol. Phys.*, 150, 245
- Karpen, J. T., Antiochos, S. K., Hohensee, M., Klimchuk, J. A., & MacNeice, P. J. 2001, *ApJ*, 553, L85
- Kim, I. S. 1990, in *Dynamics of Quiescent Prominences*, ed. V. Ruždjak & E. Tandberg-Hanssen (New York: Springer), 49
- Kim, I. S., Koutchmy, S., Stellmacher, G., & Nikolskii, G. M. 1984, *A&A*, 140, 112
- Klimchuk, J. A. 2001, in *Space Weather*, ed. P. Song, H. J. Singer, & G. Siscoe (Geophys. Monogr. 125; Washington: AGU), 143
- Kuperus, M., & Raadu, M. A. 1974, *A&A*, 31, 189
- Leroy, J. L., Bommier, V., & Sahal-Bréchet, S. 1983, *Sol. Phys.*, 83, 135
- . 1984, *A&A*, 131, 33
- Low, B. C. 1996, *Sol. Phys.* 167, 217
- Low, B. C. 2001, *J. Geophys. Res.*, 106, A11, 25,141
- Malherbe, J. M., & Priest, E. R. 1983, *A&A*, 123, 80
- Mikić, Z., & Linker, J. A. 1994, *ApJ*, 430, 898
- Nikolskii, G. M., Kim, I. S., & Koutchmy, S. 1982, *Sol. Phys.*, 81, 81
- Paletou, F., López Ariste, A., Bommier, V., & Semel, M. 2001, *A&A*, 375, L39
- Poland, A. I., & Mariska, J. T. 1986, *Sol. Phys.*, 104, 303
- Rust, D. M. 1967, *ApJ*, 150, 313
- Tandberg-Hanssen, E. 1995, *The Nature of Solar Prominences* (Dordrecht: Kluwer)
- van Ballegoijen, A. A., Priest, E. R., & MacKay, D. H. 2000, *ApJ*, 539, 983
- Zirker, J. B., Engvold, O., & Martin, S. F. 1998, *Nature*, 396, 440